

---

This is an electronic reprint of the original article.  
This reprint may differ from the original in pagination and typographic detail.

Wang, Zulin; Yliniemi, Kirsi; Wilson, Benjamin P.; Lundström, Mari

**Green and Controllable Preparation of Cu/Zn Alloys Using Combined Electrodeposition and Redox Replacement**

*Published in:*  
ACS Sustainable Chemistry and Engineering

*DOI:*  
[10.1021/acssuschemeng.2c00771](https://doi.org/10.1021/acssuschemeng.2c00771)

Published: 11/04/2022

*Document Version*  
Publisher's PDF, also known as Version of record

*Published under the following license:*  
CC BY

*Please cite the original version:*  
Wang, Z., Yliniemi, K., Wilson, B. P., & Lundström, M. (2022). Green and Controllable Preparation of Cu/Zn Alloys Using Combined Electrodeposition and Redox Replacement. *ACS Sustainable Chemistry and Engineering*, 10(14), 4770–4779. <https://doi.org/10.1021/acssuschemeng.2c00771>

---

This material is protected by copyright and other intellectual property rights, and duplication or sale of all or part of any of the repository collections is not permitted, except that material may be duplicated by you for your research use or educational purposes in electronic or print form. You must obtain permission for any other use. Electronic or print copies may not be offered, whether for sale or otherwise to anyone who is not an authorised user.

# Green and Controllable Preparation of Cu/Zn Alloys Using Combined Electrodeposition and Redox Replacement

Zulin Wang, Kirsi Yliniemi, Benjamin P. Wilson, and Mari Lundström\*

Cite This: *ACS Sustainable Chem. Eng.* 2022, 10, 4770–4779

Read Online

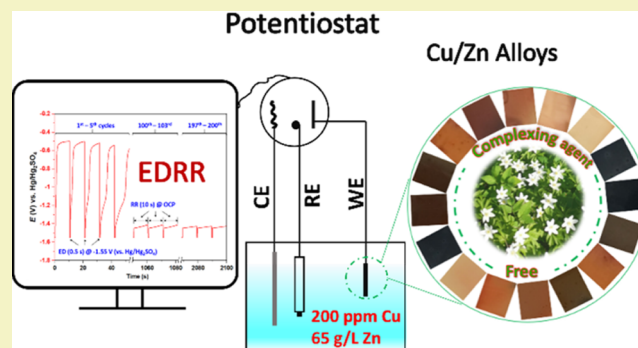
ACCESS |

Metrics &amp; More

Article Recommendations

**ABSTRACT:** This study outlines a novel and sustainable electrodeposition–redox replacement (EDRR) method to produce Cu/Zn alloys using a simulated hydrometallurgical Zn solution containing 200 ppm Cu, 65 g/L Zn, and 10 g/L H<sub>2</sub>SO<sub>4</sub>. The results indicate that by tailoring the EDRR parameters, like deposition time, replacement time, and agitation conditions, Cu/Zn alloys with controllable properties including chemical composition, microstructures, colorations, and crystalline phases can be readily obtained. Scanning electron microscopy (SEM) analysis shows that coherent Cu/Zn films grow from separate nanoscale particles produced during the initial EDRR cycles. Furthermore, the corrosion performance of the prepared Cu/Zn films is tunable by changing the crystalline phases through the variation of operating conditions. For example, deposits containing Zn-rich phases (CuZn<sub>5</sub>, Cu<sub>5</sub>Zn<sub>8</sub>) obtained with short redox replacement times without agitation resulted in relatively poor corrosion resistance. In contrast, Cu-rich phases (Cu<sub>0.75</sub>Zn<sub>0.25</sub>, Cu<sub>0.85</sub>Zn<sub>0.15</sub>) with enhanced corrosion performance were achieved with prolonged redox replacement times and/or the application of magnetic stirring. Unlike traditional electrodeposition, the EDRR method does not involve any complexing agents and the currently underutilized hydrometallurgical solutions were used as potential raw materials. Overall, the study suggests the EDRR method as a promising approach to achieve sustainable manufacturing of Cu/Zn alloys and an improved circular economy of metals.

**KEYWORDS:** cyanide-free electroplating, brass, EDRR, corrosion resistance



## INTRODUCTION

Cu/Zn alloys, also known as brass, have been used in a broad range of applications such as decoration, corrosion protection, electrode materials for energy storage, shape-memory materials, and adhesion interlayers between rubber steel tire cords.<sup>1–5</sup> Electrodeposition is one of the most common methods for Cu/Zn alloy production, nevertheless, the simultaneous deposition of Zn and Cu usually requires the addition of complexing agents due to the notable difference between the potentials of Zn<sup>2+</sup>/Zn (−0.76 V vs the standard hydrogen electrode (SHE)) and Cu<sup>2+</sup>/Cu (+0.34 V vs SHE) redox pairs. Traditionally, cyanide has been used as the complexing agent for Cu/Zn alloy electroplating,<sup>1,6,7</sup> although concerns about environmental, health, and safety issues have been escalating due to the high toxicity. Various types of complexing agents have been investigated as alternatives to cyanide, such as oxalate,<sup>8</sup> pyrophosphate,<sup>8–11</sup> ethylenediaminetetraacetic acid (EDTA),<sup>12</sup> nitrilotriacetic acid,<sup>13</sup> triethanolamine,<sup>14</sup> citrate,<sup>15,16</sup> glutamate,<sup>17</sup> gluconate,<sup>18</sup> tartrate,<sup>19</sup> sorbitol,<sup>20</sup> glycine,<sup>21</sup> and glycerol.<sup>22</sup> Nevertheless, the usage of such additives can increase the operating costs and burden of wastewater treatment.<sup>23–25</sup> Several attempts have been made

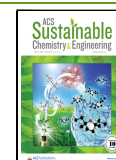
using ionic liquids and deep eutectic solvents for brass electrodeposition due to their wide electrochemical windows, vapor pressure, and high ionic conductivity,<sup>26–29</sup> however, the commercial application of these nonaqueous electrolytes has so far been limited by their high prices. On the other hand, the demand for copper and zinc has continued to increase due to the increased consumption of electronics and construction materials due to the demands of the growing global population. At the same time, the availability of high-grade raw materials has been decreasing.<sup>30,31</sup> Consequently, the utilization of secondary raw materials for brass preparation is worthy of attention as it can decrease the production cost and enhance the metal circular economy.

Recently, a novel electrodeposition–redox replacement (EDRR) method has been developed to recover valuable

Received: February 9, 2022

Revised: March 21, 2022

Published: March 30, 2022



elements such as Au,<sup>32–37</sup> Ag,<sup>32,38–40</sup> Te,<sup>41</sup> and Pt<sup>42</sup> with minute concentration (ppm or even ppb level) from different complex solutions. Moreover, the EDRR method was found to be promising for the direct production of bimetallic functional materials such as Pt/Ni,<sup>43</sup> Ag/Cu,<sup>44</sup> and Ag/Zn<sup>45</sup> particles, from industrial-type process streams. Nevertheless, previous studies have mainly focused on precious metals, while in practice, base metals can also exist as impurities in the process solutions. For instance, during the hydrometallurgical production of Zn, Cu is usually present in hundreds of ppm within the process solutions and it needs to be removed as it may contaminate the final Zn products.<sup>46</sup> However, conventional Cu removal methods like cementation,<sup>47</sup> adsorption,<sup>46</sup> and solvent extraction<sup>48,49</sup> may face challenges as the intensive usage of chemicals can increase costs and the related wastewater outputs. Moreover, additional treatments are usually needed to obtain pure Cu from the side products of these conventional processes.<sup>47</sup> Consequently, the growth of consistent Cu/Zn alloy coatings from Zn process solutions by EDRR is extremely attractive as it has been demonstrated that bimetallic particles can be prepared between metals with distinct potentials without the need for any complexing agents.<sup>43–45</sup>

This study investigates the technical feasibility of the direct production of Cu/Zn alloy films using the electrodeposition and redox replacement (EDRR) method from a hydro-metallurgical zinc process solution with 65 g/L zinc, 10 g/L H<sub>2</sub>SO<sub>4</sub>, and 200 ppm Cu as the raw materials. The whole process was conducted in a simple electrochemical cell in the absence of any types of complexing agents. The resultant Cu/Zn films were comprehensively characterized using various analytical techniques like scanning electron microscopy with energy-dispersive X-ray spectroscopy (SEM-EDS), anodic linear sweep voltammetry (ALS), X-ray diffraction (XRD), and the open-circuit potential (OCP) values. The results indicate that the properties of Cu/Zn alloy films, such as chemical composition, surface microstructures, colorations, and crystalline phases can be readily controlled by varying the operating parameters like deposition time, replacement time, and magnetic stirring. The growth protocol of the Cu/Zn films with different numbers of EDRR cycles was determined by a detailed SEM study. In addition, the corrosion performance of the Cu/Zn alloys was found to be closely related to the crystalline phases present within the films, which can be controlled by varying EDRR parameters. This further highlights the significant application potential of the Cu/Zn films obtained by the EDRR method.

## EXPERIMENTAL SECTION

All electrochemical measurements were conducted in a conventional three-electrode cell (50 cm<sup>3</sup>) and controlled using an IviumStat 24-bit CompactStat potentiostat (Ivium Technologies, Netherlands). Glassy carbon (GC) plates (one-side exposed area of 1 cm<sup>2</sup>, Alfa Aesar) were used as the working electrodes (WEs). A Pt plate (9 cm<sup>2</sup>, Pt wt % ≥99.5%, Kultakeskus Oy, Finland) was used as the counter electrode (CE) and a saturated mercury–mercurous sulfate electrode (Hg/Hg<sub>2</sub>SO<sub>4</sub>, +0.65 V vs a standard hydrogen electrode (SHE), Mettler Toledo, Switzerland) was utilized as the reference electrode (RE). The distance between the WE and CE was fixed at 2 cm. Before the electrochemical experiments, the GC electrodes were first cleaned using ethanol (≥94 wt %, Altia Oyj, Finland) in an ultrasonic bath (VWR) for 15 min, electrochemically cleaned in 0.1 M H<sub>2</sub>SO<sub>4</sub> by 10 cycles of cyclic voltammetry (CV, scan speed: 50 mV/s, potential range: −1.2 to +1.1 V), then rinsed with deionized (DI) water and

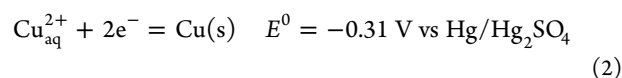
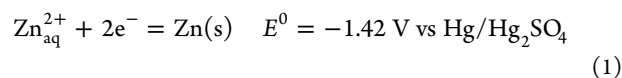
dried in air. Zn/Cu alloy films were prepared on the WE from a simulated zinc process solution (65 g/L Zn (from ZnSO<sub>4</sub>·7H<sub>2</sub>O, ≥99%, Sigma-Aldrich), 200 ppm Cu (from CuSO<sub>4</sub>·5H<sub>2</sub>O, ≥98%, Sigma-Aldrich), and 10 g/L H<sub>2</sub>SO<sub>4</sub> (from concentrated H<sub>2</sub>SO<sub>4</sub>, 95–97%, EMD Millipore)) using 200 cycles of electrodeposition–redox replacement (EDRR) at room temperature. All of the solutions were prepared with Millipore Milli-Q deionized water (DI water, ≥18 MΩ·cm).

The EDRR protocol utilizes two repetitive steps: (i) Zn is deposited at a potential of  $E_{ed}$  for a short time  $t_1$  (0.3 or 0.5 s) (ED step) and (ii) the external potential is disconnected, and the previously formed Zn deposit is replaced by Cu<sup>2+</sup> ions at the open circuit for replacement time  $t_2$  (5–40 s) (redox replacement (RR) step). Some EDRR experiments were carried out with a 100-rpm stirring speed ( $r$ ) achieved by magnetic stirring, whereas some similar samples were prepared without agitation to study the effects of mass transfer. Moreover, EDRR experiments with 2, 4, 6, 8, 15, 30, 60, and 100 cycles ( $E_{ed} = -1.55$  V (vs Hg/Hg<sub>2</sub>SO<sub>4</sub>),  $t_1 = 0.5$  s,  $t_2 = 20$  s,  $r = 100$  rpm) were conducted to study the growth process of Cu/Zn films.

Surface morphology and the composition of the deposits produced by EDRR were analyzed by scanning electron microscopy (SEM) in combination with energy-dispersive X-ray spectroscopy (EDS, ThermoFisher Scientific Ultradry EDS Detector). Results of the Cu/Zn atom percentage were average values of 5 area EDS scans per sample. Anodic linear sweep voltammetry (ALS) was performed for the Cu/Zn films in a 0.2 M (NH<sub>4</sub>)<sub>2</sub>SO<sub>4</sub> solution (from (NH<sub>4</sub>)<sub>2</sub>SO<sub>4</sub>, >99%, Alfa Aesar, Germany) at a scan speed of 5 mV/s in a potential range from −1.60 to +1.00 V (vs Hg/Hg<sub>2</sub>SO<sub>4</sub>). The crystalline phases of Cu/Zn films were determined by X-ray diffraction (XRD, PANalytical X'Pert ProPowder, Almelo, The Netherlands) using a Cu K $\alpha$  radiation source at a scan speed of 0.1°/min with a 2 $\theta$  (°) range between 15 and 90° (acceleration potential of 40 kV and current of 40 mA) and the results were analyzed using HighScore 4.0 plus software. Corrosion resistance of the Cu/Zn films was investigated by potentiodynamic polarization measurements using the same electrochemical cell as the EDRR experiments in a solution containing 3.5 wt % NaCl (from NaCl, ≥98%, Sigma-Aldrich, Germany) at room temperature. Prior to the polarization measurements, the coated samples were immersed in the NaCl solution for 30 min to achieve a stable open-circuit potential (OCP). The polarization experiments were conducted across a potential range from −350 to +350 mV (vs OCP) at a scan rate of 0.5 mV/s. The corrosion potential ( $E_{corr}$ ) and corrosion current density ( $j_{corr}$ ) were evaluated based on the Tafel extrapolation method.

## RESULTS AND DISCUSSION

**Zn/Cu Films by EDRR.** Figure 1 shows a typical potential profile as a function of time during 200 cycles of EDRR measurements. The potential–time curve of 1st–5th, 100th–103rd, and 197th–200th cycles are presented here for the purpose of clarity. As can be seen, zinc was deposited at −1.55 V (vs Hg/Hg<sub>2</sub>SO<sub>4</sub>,  $E_{ed}$ ) for 0.5 s ( $t_1$ ) via eq 1, which was immediately followed by a redox replacement step (RR) at OCP for 10 s ( $t_2$ ). The deposited zinc in the ED step was spontaneously replaced by Cu<sup>2+</sup> ions in the RR step (eq 2) due to the potential difference (1.1 V) between eqs 1 and 2.



To investigate the effects of  $t_1$ ,  $t_2$ , and agitation conditions, 16 samples (S1–S16) with different EDRR parameters were prepared with a constant  $E_{ed}$  of −1.55 V (vs Hg/Hg<sub>2</sub>SO<sub>4</sub>). The details of the experimental conditions are displayed in Table 1.

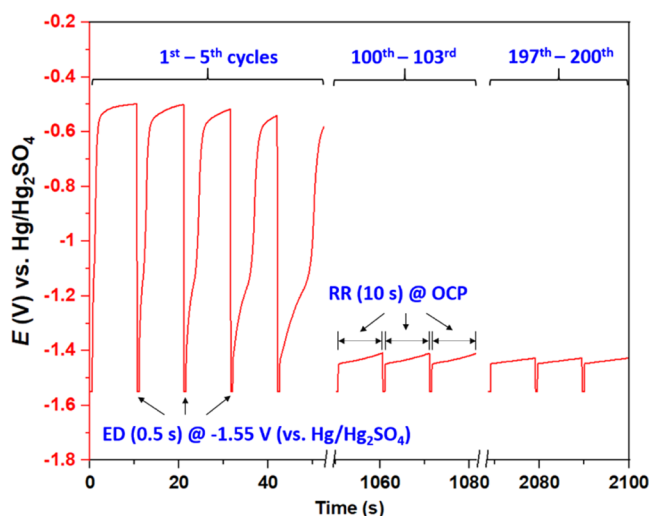


**Figure 1.** Potential–time profile during 200 cycles of EDRR measurements ( $E_{ed} = -1.55$  V (vs Hg/Hg<sub>2</sub>SO<sub>4</sub>),  $t_1 = 0.5$  s,  $t_2 = 10$  s, and  $r = 0$  rpm, for the sake of clarity, only selected cycles are presented).

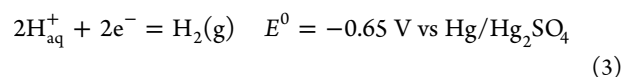
**Table 1. Parameters of EDRR Experiments and the Composition of Cu/Zn Films by EDRR (Average Value of 5 EDS Area Scans per Sample)**

sample ID	$t_1$ (s)	$t_2$ (s)	$r$ (rpm)	composition (atom %)	
				Cu	Zn
S1	0.5	5		15	85
S2	0.5	10		27	73
S3	0.5	20		65	35
S4	0.5	40		77	23
S5	0.5	5	100	67	33
S6	0.5	10	100	79	21
S7	0.5	20	100	82	18
S8	0.5	40	100	84	16
S9	0.3	5		34	66
S10	0.3	10		63	37
S11	0.3	20		72	28
S12	0.3	40		81	19
S13	0.3	5	100	80	20
S14	0.3	10	100	83	17
S15	0.3	20	100	84	16
S16	0.3	40	100	86	14

Figure 2 shows the SEM micrographs of Cu/Zn films prepared by EDRR and the related chemical compositions are also summarized in Table 1. Pure Zn and Cu metals have different electrode potentials as displayed in eqs 1 and 2, therefore, the differences in the composition of the Cu/Zn films can be characterized by the OCP values. The open-circuit potential (OCP) values at the end of each EDRR cycle were collected and are presented in Figure 3, whereas images of the samples produced by the variation in EDRR parameters are shown in Figure 4.

As can be seen from Figure 2a, spiky structures similar to the initiation of dendrite growth in traditional electrodeposition were obtained with a relatively short  $t_2 = 5$  and 10 s ( $t_1 = 0.5$  s,  $r = 0$  rpm). The formation of such morphology is related to the screw dislocation of Zn atoms deposited during the electrodeposition stage, which is affected by the limited diffusion of

Zn<sup>2+</sup> ions and hindered electron transfer.<sup>50,51</sup> The spiky structures are retained with short redox replacement step times as only a relatively low amount of Zn reacts with Cu<sup>2+</sup> and dissolves back into the solution due to the mass-transfer limitation of the copper ions that results from the low Cu concentration (200 ppm). Moreover, the notable effect of mass-transfer limitation of Cu<sup>2+</sup> ions during the redox replacement step also is reflected by the relatively low contents of Cu in the deposits when time  $t_2$  was low and the solution was not stirred (S1 and S2), as shown in Table 1. The variation of the OCP values (Figure 3a) is in accordance with the EDS results: the OCP of the first cycles showed a mixed value between the potentials of Zn and Cu metals, whereas an increase in the number of cycles resulted in a shift of the electrode potential toward more negative values close to the potential of pure Zn, which indicates the high content of Zn in the deposits. On the other hand, previously published studies have reported that the formation of spiky structures can be associated with the H<sub>2</sub> gas attached to the surface of the electrode.<sup>52,53</sup> In this study, the hydrogen evolution reaction (HER) is inevitable during the ED step as the applied potential was more negative than that outlined by eq 3. The H<sub>2</sub> formed can adsorb on the electrode surface leading to an uneven distribution of the local current density. This phenomenon also facilitates the formation of spiky structures observed with short replacement intervals due to the lack of time for gas desorption from the electrode surface to occur.



As expected, the Cu content in the deposit steadily increased with longer replacement times of 20 s (Cu 65 atom %) and 40 s (Cu 77 atom %) as more Zn was replaced by Cu ions. A dramatic change in the microstructure of the deposit was also observed when  $t_2$  increased from 10 to 20 s. A smoother surface comprised of fine particles with irregular morphology was obtained as longer replacement times allow more of the deposited Zn to react with Cu<sup>2+</sup> ions and the evolved H<sub>2</sub> to completely desorb from the electrode surface. A more compact microstructure was achieved with the further increase of  $t_2$  to 40 s. In this case, the crystal grains change to a more spherical morphology and can be seen to be more closely associated, possibly due to synergistic interaction of the increased reaction between Cu ions and Zn, H<sub>2</sub> desorption, and Ostwald ripening. The effect of the increased  $t_2$  was also reflected in the recorded OCP values for the working electrode as shown in Figure 3a. The OCP increased markedly to more positive values with longer replacement times, and this correlates with the increased Cu content within the Cu/Zn deposits. Additionally, the coloration of the brass films was found to be related to the Cu/Zn ratios as well as the surface morphology and these can be readily altered by tailoring the EDRR parameters. A notable variation of surface coloration with different  $t_2$  values was observed as shown in Figure 4a. Initially, dark gray deposits were obtained at  $t_2$  of 5 s (S1) and 10 s (S2) due to the high Zn content, whereas the deposit with a  $t_2$  value of 20 s (S3) appeared brown and this was subsequently observed to change to a more copper color when  $t_2$  was further increased to 40 s (S4).

A clear difference in the morphology was observed when magnetic stirring (100 rpm) was applied (see Figure 2b). Instead of spiky structures, for S5 ( $t_2 = 5$  s) the surface morphology was found to comprise of small flakes, whereas

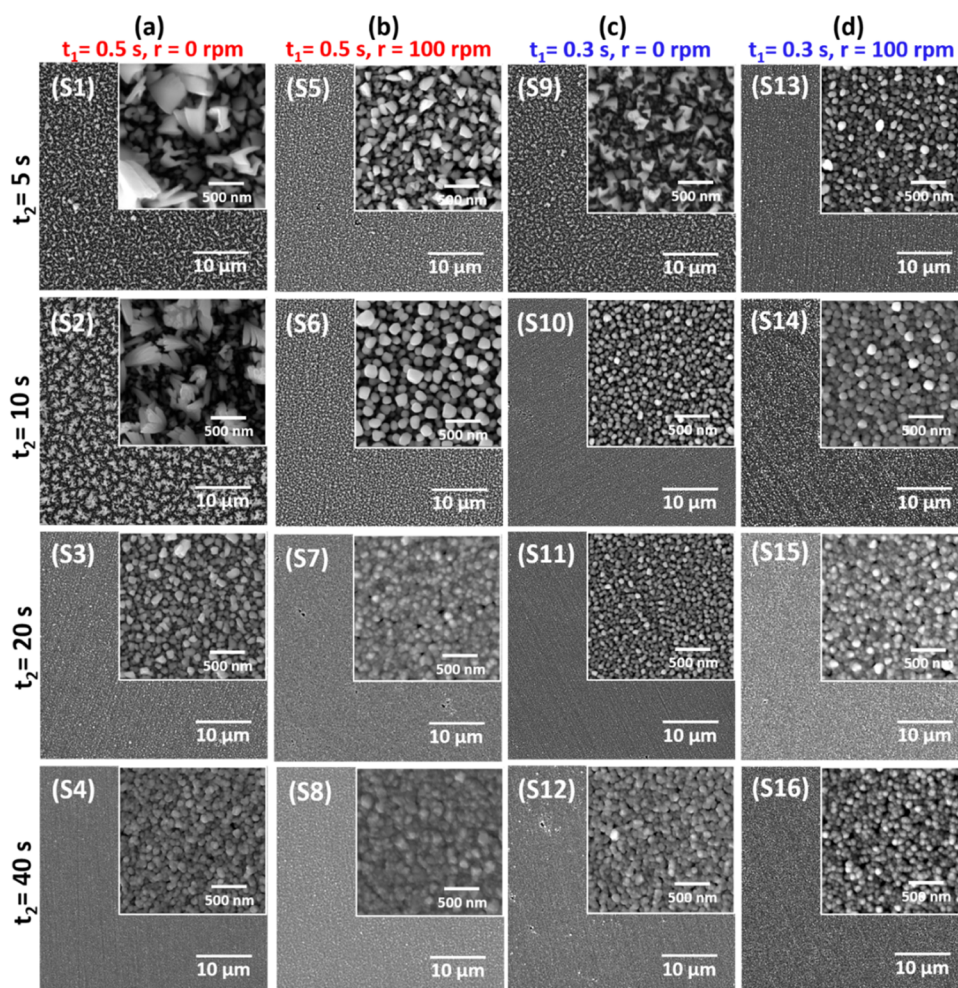


**Figure 2.** SEM micrographs of Cu/Zn alloys from a solution containing 200 ppm Cu, 65 g/L Zn, and 10 g/L  $\text{H}_2\text{SO}_4$  by 200 EDRR cycles. (a)  $t_1 = 0.5$  s,  $t_2 = 5\text{--}40$  s,  $r = 0$  rpm; (b)  $t_1 = 0.5$  s,  $t_2 = 5\text{--}40$  s,  $r = 100$  rpm; (c)  $t_1 = 0.3$  s,  $t_2 = 5\text{--}40$  s,  $r = 0$  rpm; and (d)  $t_1 = 0.3$  s,  $t_2 = 5\text{--}40$  s,  $r = 100$  rpm.

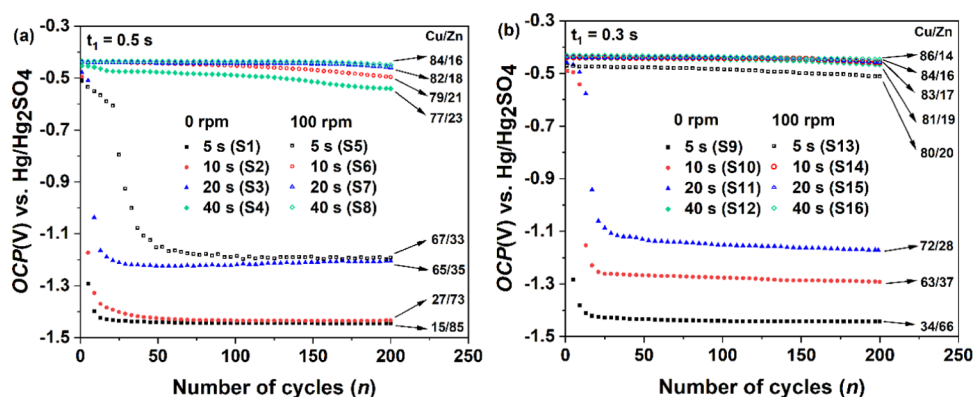


**Figure 3.** Open-circuit potential (OCP) values at the ends of the EDRR cycles during the preparation of samples (a) S1–S8,  $t_1 = 0.5$  s and (b) S9–S16,  $t_1 = 0.3$  s.

with a longer  $t_2$  of 10 s (S6) a surface structure with a loose structure of fine particles was evidence. This can be ascribed to the fact that agitation greatly improved not only the diffusion conditions for Zn ions in the ED step and Cu ions during the RR step but also the desorption of  $\text{H}_2$ . Compared to the Cu content within samples S1 (15 atom %) and S2 (27 atom %), the Cu content within S5 and S6 increased to 67 and 79 atom %, respectively. Also, with a replacement time of 5 s (S5) and

10 s (S6), the OCP values of the working electrode are more positive than that of S1 and S2, which agrees with the higher Cu within the samples as a result of stirring. With further increased replacement times (S7 and S8), more compact structures were obtained which were similar to the surfaces produced without agitation, although the changes in the Cu content and OCP values are less considerable. The variation of the chemical composition is also reflected in the sample

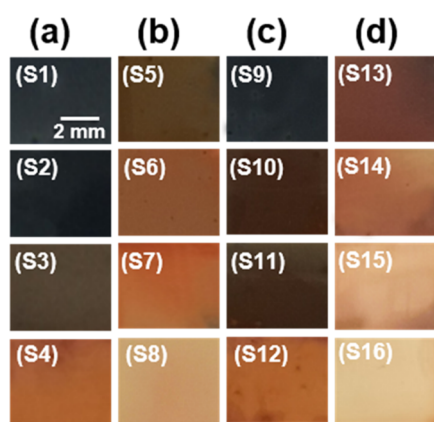


**Figure 4.** Photos of Cu/Zn alloys from a solution containing 200 ppm Cu, 65 g/L Zn, and 10 g/L  $\text{H}_2\text{SO}_4$  by 200 EDRR cycles. (a)  $t_1 = 0.5$  s,  $t_2 = 5$ –40 s,  $r = 0$  rpm; (b)  $t_1 = 0.5$  s,  $t_2 = 5$ –40 s,  $r = 100$  rpm; (c)  $t_1 = 0.3$  s,  $t_2 = 5$ –40 s,  $r = 0$  rpm; and (d)  $t_1 = 0.3$  s,  $t_2 = 5$ –40 s,  $r = 100$  rpm.

coloration (Figure 4b), which vary from brown, through brown/orange, to medium orange, and bright yellow when  $t_2$  was increased from 5 to 40 s.

The effect of deposition time was further investigated by the use of a shorter  $t_1 = 0.3$  s. As can be seen from Figure 2c, the sample prepared with this time and  $t_2 = 5$  s (S9) also has a spiky microstructure. Nevertheless, a drastic change in the surface product morphology (i.e., from spiky structure to smooth surface) was still observed and more compact microstructures were achieved by further increasing the replacement time. In this case, where  $t_1 = 0.3$  s, the diffusion limitation in the ED step is less severe due to the lower consumption of Zn ions in the vicinity of the electrode and reduced level of zinc deposited on the surface. Consequently, a shorter replacement time  $t_2 = 10$  s (S10) was needed when  $t_1 = 0.3$  s for the morphology transition cf., 20 s (when  $t_1 = 0.5$  s, S3). On the other hand, when  $t_1 = 0.3$  s less  $\text{H}_2$  gas is generated, which may also lessen the formation of a spiky structure. In addition, it can be observed that the grain size shown in Figure 2a (S1–S4) is discernably larger than that in Figure 2c (S9–S12), as a longer  $t_1$  of 0.5 s allows the nucleation points formed during the initial stage to grow<sup>54</sup> and a similar phenomenon has also been reported during the formation of Ag/Cu particles by EDRR.<sup>44</sup> The effect of the deposition time is reflected by the variation of the chemical

composition of the deposits and the working electrode OCP values. With the same replacement time, the Cu percentage for samples with  $t_1 = 0.3$  s is markedly higher than those where  $t_1 = 0.5$  s. For example, compared to S1 (Cu 15 atom %), the Cu content within S9 increased to 34 atom %. Accordingly, the OCP values recorded when  $t_1 = 0.3$  s (S10–S12, Figure 3b) are, in general, more positive when compared to those from S2–S4 where the same  $t_2$  (10–40 s) was applied. In contrast, for the samples produced by  $t_2 = 5$  s, the Cu content within S9 is higher than S1 even though the OCP values were found to be similar. This could be attributed to the presence of Zn-rich brass phases, which means there is still a considerable amount of Zn within both samples. The dark gray color observed for S9 results from the high zinc content and the coloration of the samples was found to change to a more copper-like appearance with the increase in  $t_2$  from 10 to 40 s (Figure 4c).

Moreover, the notable improvement in the mass-transfer process by agitation is still observed for the samples where  $t_1 = 0.3$  s. As shown in Figure 2d, no spiky structure formation is evident for the sample where  $t_2 = 5$  s when 100 rpm magnetic stirring is applied. The recorded OCP is also in accordance with the deposit composition as the working electrode OCP for  $t_2 = 5$ –20 s had significantly higher values compared to those in the absence of agitation (Figure 3b). Also, the Cu/Zn ratio was considerably higher when no stirring was applied, resulting in a range of colors from red through brown to yellow, as shown in Figure 4d.

Figure 5 shows the anodic linear sweep voltammetry (ALS) results. Different oxidation peaks were observed during the potentiodynamic scans of the Cu/Zn films obtained by various EDRR parameters and these potential peaks are directly related to the crystalline phases present in the Cu/Zn alloys. To further identify the crystalline phases of the Cu/Zn films, the deposits were further characterized by X-ray diffraction (XRD) as displayed in Figure 6. For samples S1 and S2 ( $t_1 = 0.5$  s,  $r = 0$  rpm,  $t_2 = 5$  and 10 s, respectively) and three peaks ( $a_1$ ,  $a_2$ ,  $a_3$ ) were observed. Based on the XRD results in Figure 6a, peak  $a_1$  can be associated with the dissolution of the Zn component from a  $\text{CuZn}_5$  alloy present in these samples. Peak  $a_2$ , located at a more positive potential, can be attributed to the dissolution of Zn from another alloy phase with higher Cu content ( $\text{Cu}_5\text{Zn}_8$ ). Although  $a_2$  was observed for both S1 and S2, the XRD peaks related to  $\text{Cu}_5\text{Zn}_8$  are not visible within the XRD spectrum of S1. The reasonable explanation is that, for S1,  $\text{Cu}_5\text{Zn}_8$  was generated after the

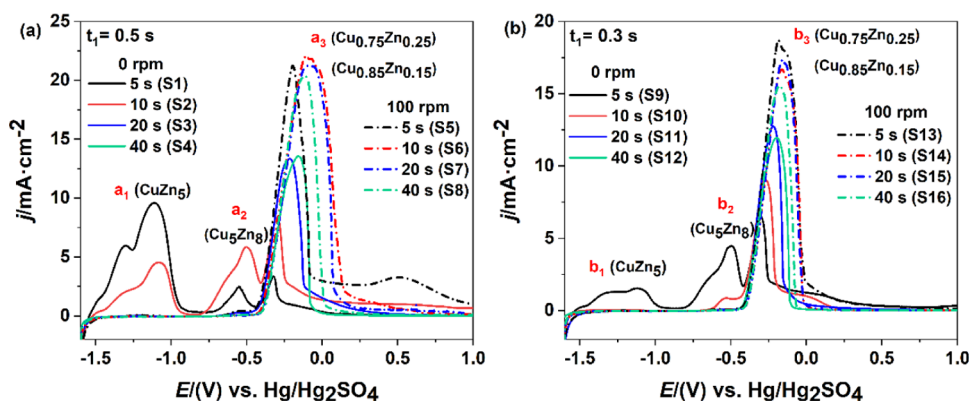


**Figure 5.** Anodic linear sweep voltammetry (ALS) curves of Cu/Zn samples by EDRR in a 0.2 M  $(\text{NH}_4)_2\text{SO}_4$  solution: (a) S1–S8,  $t_1 = 0.5$  s and (b) S9–S16,  $t_1 = 0.3$  s.

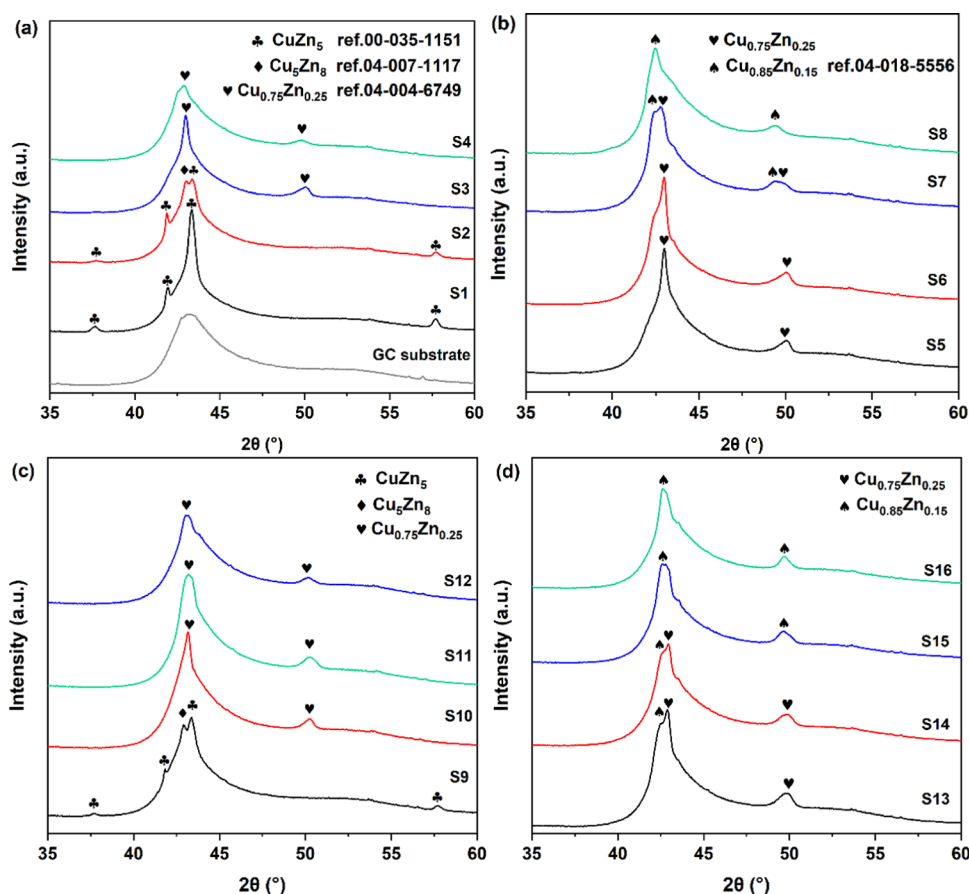


Figure 6. XRD patterns of ED RR samples: (a) S1–S4, (b) S5–S8, (c) S9–S12, and (d) S13–S16.

dissolution of the Zn component from the  $\text{CuZn}_5$  phase, while for S2, both crystalline phases ( $\text{Cu}_5\text{Zn}_8$  and  $\text{CuZn}_5$ ) were formed during sample preparation. For the samples with longer replacement times (S3 and S4), only a single peak ( $a_3$ ) was detected during ALSV measurements. According to the XRD results, peak  $a_3$  within these samples is related to a Cu-rich intermetallic ( $\text{Cu}_{0.75}\text{Zn}_{0.25}$ ).

In contrast, when magnetic stirring was applied during ED RR (S5–S8), all of the ALSV curves showed only a single oxidation peak. The related XRD results (Figure 6b) indicate that S5 and S6 are mainly comprised of  $\text{Cu}_{0.75}\text{Zn}_{0.25}$ . With an increase in  $t_2$  to 20 s (S7), more Zn was replaced by Cu and, therefore, another Cu-rich phase ( $\text{Cu}_{0.85}\text{Zn}_{0.15}$ ) was found to be present. For the longest replacement investigated ( $t_2 = 40$  s, S8), the predominant phase was found to consist of  $\text{Cu}_{0.85}\text{Zn}_{0.15}$ . Interestingly, the dissolution of  $\text{Cu}_{0.85}\text{Zn}_{0.15}$  and  $\text{Cu}_{0.75}\text{Zn}_{0.25}$  did not appear in the ALSV as separate anodic peaks, possibly because these two phases have similar oxidation potentials.

For sample S9 ( $t_1 = 0.3$  s,  $r = 0$  rpm,  $t_2 = 5$  s), three peaks ( $b_1$ ,  $b_2$ ,  $b_3$ ) were observed as shown in Figure 5b and two crystalline phases were identified in the corresponding XRD patterns (Figure 6c). For samples S10–S12, single-peak ALSV curves were obtained, which correlates with the Cu-rich phase ( $\text{Cu}_{0.75}\text{Zn}_{0.25}$ ) present within these samples. The replacement time needed to obtain the Cu-rich phase when  $t_1 = 0.3$  s was somewhat shorter than that for  $t_1 = 0.5$  s (10 s cf. 20 s; S10 and S2), a finding that correlates with the EDS results in Table 1. In comparison, for samples S13–S16, only one peak ( $b_3$ ) was observed in the ALSV curves, nevertheless, according to the

associated XRD patterns—shown in Figure 6d—the dominant crystalline phases within these samples were as follows: S13 ( $\text{Cu}_{0.75}\text{Zn}_{0.25}$ ,  $\text{Cu}_{0.85}\text{Zn}_{0.15}$ ), S14 ( $\text{Cu}_{0.75}\text{Zn}_{0.25}$ ,  $\text{Cu}_{0.85}\text{Zn}_{0.15}$ ), S15 ( $\text{Cu}_{0.85}\text{Zn}_{0.15}$ ), and S16 ( $\text{Cu}_{0.85}\text{Zn}_{0.15}$ ).

Figure 7 shows the evolution of the morphology of the Cu/Zn film as a function of the number of ED RR cycles (ED RR parameters:  $t_1 = 0.5$  s,  $t_2 = 20$  s,  $r = 100$  rpm). As can be seen from Figure 7a, separated nanoparticles with an average diameter of  $31 \pm 16$  nm were already formed on the substrate after 2 ED RR cycles. In general, the size of the particles is smaller than the cluster size ( $<10$  nm) formed in the initial cycles by surface-limited redox replacement (SLRR). Such an observation probably is because SLRR uses sacrificial layers formed by underpotential deposition, whereas the ED RR methodology used in this study involved Zn deposition at its bulk potential range.<sup>55–60</sup> When the number of cycles was increased from 2 to 10 cycles, a steady increase of the particle size was observed and the boundaries between particles can be clearly identified, such a trend has also been reported for Pt/Ni and Ag/Zn particle preparation by ED RR.<sup>43,45</sup> After 15 cycles, the particles continue to grow and individual particles begin to coalesce with each other as shown in Figure 7f. Finally, an almost complete surface layer comprising of associated spherical particles is formed when the more than 60 ED RR cycles were repeated (Figure 7h,i). This mechanism of growth—from individual particles to a continuous layer—has also been commonly observed during the deposition of metal layers by SLRR and is associated with the surface energy and the surface mobility of metal atoms.<sup>56,59,61</sup>

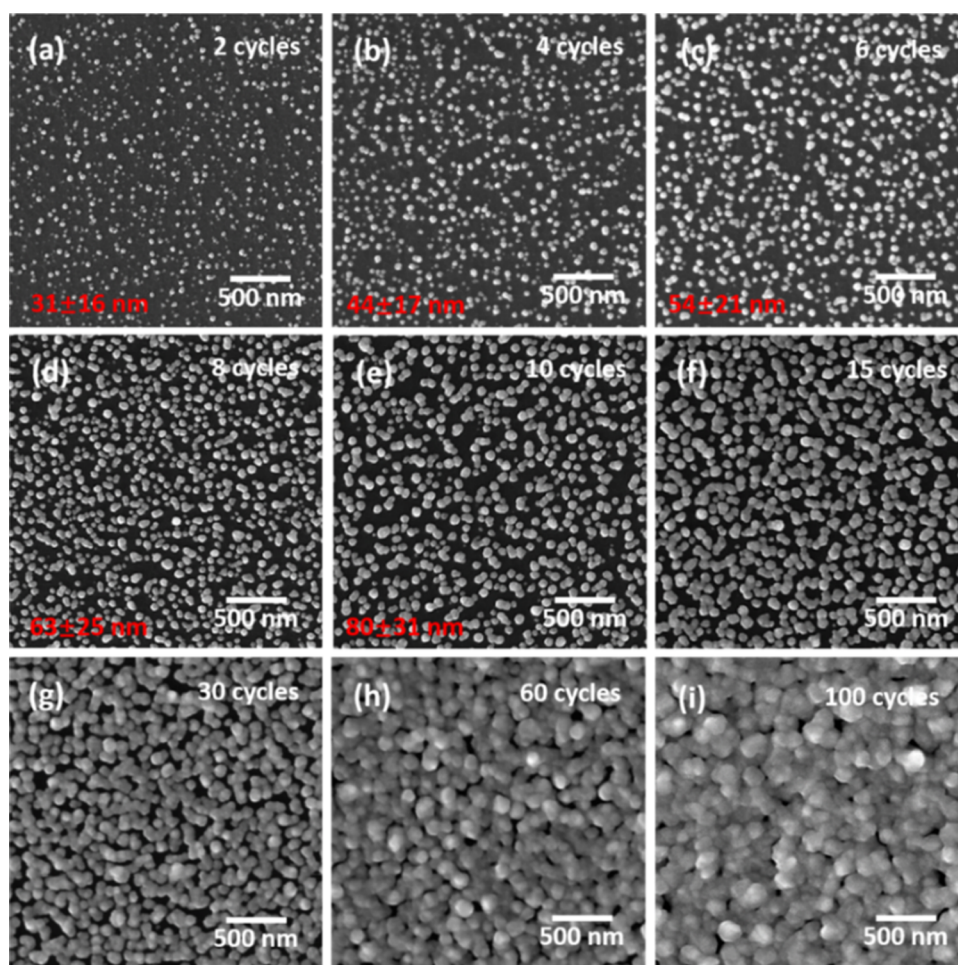


**Figure 7.** SEM images of the GC working electrode surface after different number of EDRC cycles: (a) 2, (b) 4, (c) 6, (d) 8, (e) 10, (f) 15, (g) 30, (h) 60, and (i) 100 cycles ( $E_{ed} = -1.55$  V,  $t_1 = 0.5$  s,  $t_2 = 20$  s,  $r = 100$  rpm).

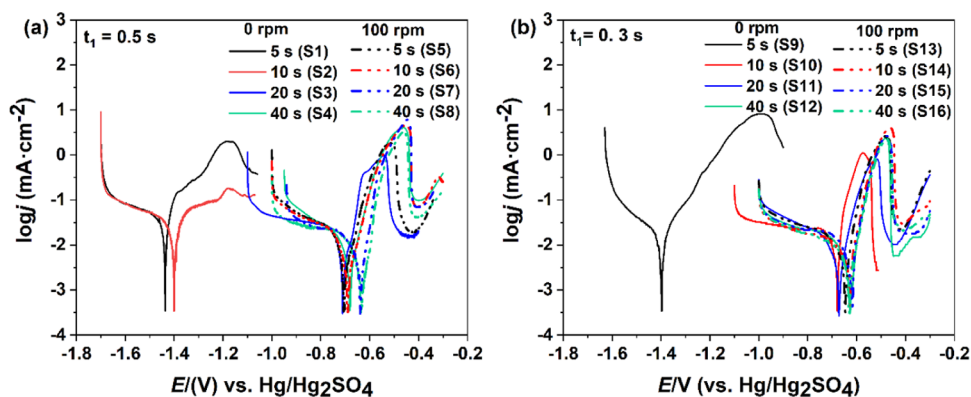


**Figure 8.** Potentiodynamic polarization curves of the Cu/Zn samples by EDRC in a 3.5 wt % NaCl solution: (a) S1–S8,  $t_1 = 0.5$  s and (b) S9–S16,  $t_1 = 0.3$  s.

**Corrosion Performance.** Corrosion performance of the Cu/Zn surface films was investigated via potentiodynamic polarization tests by the Tafel method as shown in Figure 8. Moreover, the associated corrosion potentials ( $E_{corr}$ ) and corrosion current densities ( $j_{corr}$ ) determined by Tafel extrapolation are summarized in Table 2. Generally, the corrosion performance of the EDRC deposited Cu/Zn films is closely related to the phase composition. For example, samples produced by a short replacement time without stirring (S1, S2, and S8) have a markedly more negative  $E_{corr}$  (between  $-1.39$

and  $-1.44$  V vs Hg/Hg<sub>2</sub>SO<sub>4</sub>) and higher  $J_{corr}$  ( $10.9$ – $25.7$   $\mu\text{A}/\text{cm}^2$ ), which indicates a lower corrosion resistance when compared to other samples. Such a low corrosion resistance results from the presence of the CuZn<sub>5</sub> phase within these samples and a similar corrosion behavior has been reported previously for Zn-rich phases in Cu/Zn coatings produced by traditional electrodeposition (ED) from a deep eutectic solvent (mixture of ChCl and urea in a molar ratio of 1:2) as shown in Table 2.<sup>26,29</sup> In contrast, this study shows that Cu/Zn coatings with tunable corrosion resistance can be obtained from

**Table 2. Corrosion Characteristics of Cu/Zn Alloy Films Summarized from Potentiodynamic Polarization Tests in 3.5 wt % NaCl Solution**

sample ID	$E_{\text{corr}}$ (mV) vs Hg/Hg <sub>2</sub> SO <sub>4</sub>	$J_{\text{corr}}$ ( $\mu\text{A}/\text{cm}^2$ )
S1	-1442	25.7
S2	-1403	16.2
S3	-701	5.3
S4	-672	3.9
S5	-693	4.2
S6	-672	3.4
S7	-634	3.2
S8	-625	3.2
S9	-1385	10.9
S10	-668	7.8
S11	-662	4.2
S12	-624	3.7
S13	-628	4.3
S14	-631	3.9
S15	-619	3.6
S16	-632	3.3
by ED from ChCl/urea mixture <sup>26</sup>	-1270 to -831	1.9–12.2
by ED from ChCl/urea mixture <sup>29</sup>	-1533 to -1094	12.1–63.5
by ED from sulfate/chloride solutions containing trisodium citrate <sup>16</sup>	-1001 to -901	19.0–42.0

aqueous solution through control of the applied EDRR parameters. When no agitation was applied to the system, the corrosion performance can be markedly improved by increasing the redox replacement time. For instance, the  $E_{\text{corr}}$  of S4 ( $t_2 = 40$  s) increased to  $-0.67$  V while the  $j_{\text{corr}}$  decreased to  $3.9 \mu\text{A}/\text{cm}^2$  cf. to  $E_{\text{corr}} = -1.44$  V and  $j_{\text{corr}} > 25.0 \mu\text{A}/\text{cm}^2$  for S1.

When stirring was applied, the replacement time required to achieve improved corrosion resistance was determined to be clearly shorter. All  $J_{\text{corr}}$  values for samples produced with agitation were less than  $4 \mu\text{A}/\text{cm}^2$  when the replacement time was  $>10$  s (S6–S8, S13–S16), and these values are similar to those for Cu-rich Cu/Zn coatings produced by electrodeposition from a relatively expensive deep eutectic solvent.<sup>26</sup> Additionally, a slight improvement in corrosion resistance was also observed for the samples which had both a longer replacement and stirring time, which is probably due to the formation of more compact microstructures. Compared with the previous Cu/Zn films by traditional electrodeposition from sulfate/chloride solutions using trisodium citrate as the complexing agent,<sup>16</sup> the Cu/Zn films by EDRR also showed enhanced corrosion behavior as presented in Table 2.

## CONCLUSIONS

Cu/Zn alloys were successfully prepared from a simulated hydrometallurgical zinc process solution (200 ppm Cu, 65 g/L Zn and 10 g/L H<sub>2</sub>SO<sub>4</sub>) using the electrodeposition–redox replacement (EDRR) method based on the spontaneous replacement of pulsed-deposited Zn by Cu<sup>2+</sup> ions in the solution. The morphology, chemical composition, and crystalline phases of the deposited Cu/Zn alloys can be controlled by tailoring the EDRR parameters like deposition potential ( $E_1$ ), deposition time ( $t_1$ ), redox replacement time ( $t_2$ ), and the presence or absence of stirring. Due to the low concentration of Cu (200 ppm), the mass-transfer limitation has significant effects on the properties of the deposits.

Samples with a short replacement time without agitation have spiky structures with high Zn content and Zn-rich phases (CuZn<sub>5</sub> or CuZn<sub>5</sub> + Cu<sub>5</sub>Zn<sub>8</sub>). By increasing the replacement time or through the application of magnetic stirring, the Cu/Zn films can be tuned to be smooth structures with high Cu content that comprise of Cu-rich phases (Cu<sub>0.75</sub>Zn<sub>0.25</sub> or Cu<sub>0.75</sub>Zn<sub>0.25</sub> + Cu<sub>0.85</sub>Zn<sub>0.15</sub> or Cu<sub>0.85</sub>Zn<sub>0.15</sub>). Consequently, the corrosion performance of the Cu/Zn alloys is also controllable through the variation of the EDRR parameters as the corrosion resistance is directly related to the types of crystalline phases present. Compared to the traditional electrodeposition, currently underutilized secondary raw materials, like hydrometallurgical process solutions, could be used with the EDRR method to form corrosion-resistant Cu/Zn surfaces without the need for additional complexing agents, which can decrease both the costs and environmental burden associated with current brass alloy manufacturing processes.

## AUTHOR INFORMATION

### Corresponding Author

Mari Lundström – Department of Chemical and Metallurgical Engineering, School of Chemical Engineering, Aalto University, 02150 Espoo, Finland; Email: mari.lundstrom@aalto.fi

### Authors

Zulin Wang – Department of Chemical and Metallurgical Engineering, School of Chemical Engineering, Aalto University, 02150 Espoo, Finland; [orcid.org/0000-0002-2234-7983](https://orcid.org/0000-0002-2234-7983)

Kirsi Yliniemi – Department of Chemistry and Materials Science, School of Chemical Engineering, Aalto University, 02150 Espoo, Finland; [orcid.org/0000-0003-2536-388X](https://orcid.org/0000-0003-2536-388X)

Benjamin P. Wilson – Department of Chemical and Metallurgical Engineering, School of Chemical Engineering, Aalto University, 02150 Espoo, Finland; [orcid.org/0000-0002-2874-6475](https://orcid.org/0000-0002-2874-6475)

Complete contact information is available at: <https://pubs.acs.org/10.1021/acssuschemeng.2c00771>

### Notes

The authors declare no competing financial interest. The data underlying this study are openly available in Zenodo at 10.5281/zenodo.5674894.

## ACKNOWLEDGMENTS

Academy of Finland project (GoldTail (319691) K.L., B.P.W) and EARMetal (339979, M.L.) are greatly acknowledged for funding this research. The RawMatTERS Finland Infrastructure (RAMI) funded by Academy of Finland and based at Aalto University is also acknowledged. In addition, Z.W. appreciates the financial support from Chinese Scholarship Council (Grant No. 201706370244) and Finnish Foundation for Technology Promotion (Grant No. 8188).

## REFERENCES

- Brenner, A. *Electrodeposition of Alloys: Principles and Practice*; Academic Press, 1967.
- Milošev, I.; Mikić, T. K.; Gaberšček, M. The Effect of Cu-Rich Sub-Layer on the Increased Corrosion Resistance of Cu–XZn Alloys in Chloride Containing Borate Buffer. *Electrochim. Acta* **2006**, *52*, 415–426.

- (3) Varzi, A.; Mattarozzi, L.; Cattarin, S.; Guerriero, P.; Passerini, S. 3D Porous Cu–Zn Alloys as Alternative Anode Materials for Li-Ion Batteries with Superior Low T Performance. *Adv. Energy Mater.* **2018**, *8*, No. 1701706.
- (4) Karahan, İH.; Özdemir, R. Effect of Cu Concentration on the Formation of Cu<sub>1-x</sub>Zn<sub>x</sub> Shape Memory Alloy Thin Films. *Appl. Surf. Sci.* **2014**, *318*, 100–104.
- (5) Ozawa, K.; Kakubo, T.; Shimizu, K.; Amino, N.; Mase, K.; Komatsu, T. High-Resolution Photoelectron Spectroscopy Analysis of Sulfidation of Brass at the Rubber/Brass Interface. *Appl. Surf. Sci.* **2013**, *264*, 297–304.
- (6) Fujiwara, Y.; Enomoto, H. Electrodeposition of B'-Brass from Cyanide Baths with Accumulative Underpotential Deposition of Zn. *J. Electrochem. Soc.* **2000**, *147*, 1840–1846.
- (7) Pan, L. C. Complex Cyanides in Brass Plating Solutions. *Trans. Electrochem. Soc.* **1932**, *62*, No. 63.
- (8) Despić, A. R.; Marinović, V.; Jović, V. D. Kinetics of Deposition and Dissolution of Brass from the Pyrophosphate–Oxalate Bath. *J. Electroanal. Chem.* **1992**, *339*, 473–488.
- (9) Johannsen, K.; Page, D.; Roy, S. A Systematic Investigation of Current Efficiency during Brass Deposition from a Pyrophosphate Electrolyte Using RDE, RCE, and QCM. *Electrochim. Acta* **2000**, *45*, 3691–3702.
- (10) Senna, L. F.; Díaz, S. L.; Sathler, L. Electrodeposition of Copper–Zinc Alloys in Pyrophosphate-Based Electrolytes. *J. Appl. Electrochem.* **2003**, *33*, 1155–1161.
- (11) Vivegnis, S.; Krid, M.; Delhalle, J.; Mekhalif, Z.; Renner, F. U. Use of Pyrophosphate and Boric Acid Additives in the Copper–Zinc Alloy Electrodeposition and Chemical Dealloying. *J. Electroanal. Chem.* **2019**, *848*, No. 113310.
- (12) de Almeida, M. R. H.; Barbano, E. P.; Zacarin, M. G.; de Brito, M. M.; Tulio, P. C.; Carlos, I. A. Electrodeposition of CuZn Films from Free-of-Cyanide Alkaline Baths Containing EDTA as Complexing Agent. *Surf. Coat. Technol.* **2016**, *287*, 103–112.
- (13) Krishnan, R. M.; Muralidharan, V. S.; Natarajan, S. R. A Non-Cyanide Brass Plating Bath. *Bull. Electrochem.* **1996**, *12*, 274–277.
- (14) Vivegnis, S.; Delhalle, J.; Mekhalif, Z.; Renner, F. U. Copper–Zinc Alloy Electrodeposition Mediated by Triethanolamine as a Complexing Additive and Chemical Dealloying. *Electrochim. Acta* **2019**, *319*, 400–409.
- (15) Ferreira, F. B. A.; Silva, F. L. G.; Luna, A. S.; Lago, D. C. B.; Senna, L. F. Response Surface Modeling and Optimization to Study the Influence of Deposition Parameters on the Electrodeposition of Cu–Zn Alloys in Citrate Medium. *J. Appl. Electrochem.* **2007**, *37*, 473–481.
- (16) Oulmas, C.; Mameri, S.; Boughrara, D.; Kadri, A.; Delhalle, J.; Mekhalif, Z.; Benfedda, B. Comparative Study of Cu–Zn Coatings Electrodeposited from Sulphate and Chloride Baths. *Heliyon* **2019**, *5*, No. e02058.
- (17) Ibrahim, M. A. M.; Bakdash, R. S. Copper-Rich Cu–Zn Alloy Coatings Prepared by Electrodeposition from Glutamate Complex Electrolyte: Morphology, Structure, Microhardness and Electrochemical Studies. *Surf. Interfaces* **2020**, *18*, No. 100404.
- (18) Survila, A.; Mockus, Z.; Kanapekaitė, S.; Stalnionis, G. Kinetics of Zinc and Copper Reduction in Gluconate–Sulfate Solutions. *Electrochim. Acta* **2013**, *94*, 307–313.
- (19) Domínguez-Ríos, C.; Moreno, M. V.; Torres-Sánchez, R.; Antúnez, W.; Aguilar-Elguézabal, A.; González-Hernández, J. Effect of Tartrate Salt Concentration on the Morphological Characteristics and Composition of Cu–Zn Electroless Plating on Zamak 5 Zinc Alloy. *Surf. Coat. Technol.* **2008**, *202*, 4848–4854.
- (20) de Almeida, M. R. H.; Barbano, E. P.; de Carvalho, M. F.; Tulio, P. C.; Carlos, I. A. Copper–Zinc Electrodeposition in Alkaline-Sorbitol Medium: Electrochemical Studies and Structural, Morphological and Chemical Composition Characterization. *Appl. Surf. Sci.* **2015**, *333*, 13–22.
- (21) Rashwan, S. M. Electrodeposition of Zn–Cu Coatings from Alkaline Sulphate Bath Containing Glycine. *Trans. IMF* **2007**, *85*, 217–224.
- (22) Das, S.; Jena, S.; Banthia, S.; Mitra, A.; Das, S.; Das, K. Novel Pulse Potentiostatic Electrodeposition Route for Obtaining Pure Intermetallic Cu<sub>5</sub>Zn<sub>8</sub>-CuZn Composite Coating Using Glycerol-NaOH Based Electrolyte with Advanced Scratch Resistance and Anti-Corrosive Properties. *J. Alloys Compd.* **2019**, *792*, 770–779.
- (23) Barros, K. S.; Espinosa, D. C. R. Chronopotentiometry of an Anion-Exchange Membrane for Treating a Synthesized Free-Cyanide Effluent from Brass Electrodeposition with EDTA as Chelating Agent. *Sep. Purif. Technol.* **2018**, *201*, 244–255.
- (24) Fu, D.; Kurniawan, T. A.; Avtar, R.; Xu, P.; Othman, M. H. D. Recovering Heavy Metals from Electroplating Wastewater and Their Conversion into Zn<sub>2</sub>Cr-Layered Double Hydroxide (LDH) for Pyrophosphate Removal from Industrial Wastewater. *Chemosphere* **2021**, *271*, No. 129861.
- (25) Barros, K. S.; Scarazzato, T.; Pérez-Herranz, V.; Espinosa, D. C. R. Treatment of Cyanide-Free Wastewater from Brass Electrodeposition with EDTA by Electrodialysis: Evaluation of Underlimiting and Overlimiting Operations. *Membranes* **2020**, *10*, No. 69.
- (26) Xie, X.; Zou, X.; Lu, X.; Xu, Q.; Lu, C.; Chen, C.; Zhou, Z. Electrodeposition Behavior and Characterization of Copper–Zinc Alloy in Deep Eutectic Solvent. *J. Appl. Electrochem.* **2017**, *47*, 679–689.
- (27) De Vreese, P.; Skoczylas, A.; Matthijs, E.; Fransaeer, J.; Binnemans, K. Electrodeposition of Copper–Zinc Alloys from an Ionic Liquid-like Choline Acetate Electrolyte. *Electrochim. Acta* **2013**, *108*, 788–794.
- (28) Rousse, C.; Beaufils, S.; Fricoteaux, P. Electrodeposition of Cu–Zn Thin Films from Room Temperature Ionic Liquid. *Electrochim. Acta* **2013**, *107*, 624–631.
- (29) Xie, X.; Zou, X.; Lu, X.; Lu, C.; Cheng, H.; Xu, Q.; Zhou, Z. Electrodeposition of Zn and Cu–Zn Alloy from ZnO/CuO Precursors in Deep Eutectic Solvent. *Appl. Surf. Sci.* **2016**, *385*, 481–489.
- (30) Ng, K. S.; Head, I.; Premier, G. C.; Scott, K.; Yu, E.; Lloyd, J.; Sadhukhan, J. A Multilevel Sustainability Analysis of Zinc Recovery from Wastes. *Resour., Conserv. Recycl.* **2016**, *113*, 88–105.
- (31) Brar, K. K.; Magdoui, S.; Etteieb, S.; Zolfaghari, M.; Fathollahzadeh, H.; Calugaru, L.; Komtchou, S.-P.; Tanabene, R.; Brar, S. K. Integrated Bioleaching-Electrometallurgy for Copper Recovery - A Critical Review. *J. Cleaner Prod.* **2021**, *291*, No. 125257.
- (32) Yliniemi, K.; Wang, Z.; Korolev, I.; Hannula, P.; Halli, P.; Lundström, M. Effect of Impurities in Precious Metal Recovery by Electrodeposition-Redox Replacement Method from Industrial Side-Streams and Process Streams. *ECS Trans.* **2018**, *85*, No. 59.
- (33) Korolev, I.; Altinkaya, P.; Haapalainen, M.; Kolehmainen, E.; Yliniemi, K.; Lundström, M. Electro-Hydrometallurgical Chloride Process for Selective Gold Recovery from Refractory Telluride Gold Ores: A Mini-Pilot Study. *Chem. Eng. J.* **2022**, *429*, No. 132283.
- (34) Korolev, I.; Altinkaya, P.; Halli, P.; Hannula, P.-M.; Yliniemi, K.; Lundström, M. Electrochemical Recovery of Minor Concentrations of Gold from Cyanide-Free Cupric Chloride Leaching Solutions. *J. Cleaner Prod.* **2018**, *186*, 840–850.
- (35) Altinkaya, P.; Wang, Z.; Korolev, I.; Hamuyuni, J.; Haapalainen, M.; Kolehmainen, E.; Yliniemi, K.; Lundström, M. Leaching and Recovery of Gold from Ore in Cyanide-Free Glycine Media. *Miner. Eng.* **2020**, *158*, No. 106610.
- (36) Korolev, I.; Spathariotis, S.; Yliniemi, K.; Wilson, B. P.; Abbott, A. P.; Lundström, M. Mechanism of Selective Gold Extraction from Multi-Metal Chloride Solutions by Electrodeposition-Redox Replacement. *Green Chem.* **2020**, *22*, 3615–3625.
- (37) Korolev, I.; Yliniemi, K.; Lindgren, M.; Carpen, L.; Lundström, M. Performance-Based Selection of the Cathode Material for the Electrodeposition-Redox Replacement Process of Gold Recovery from Chloride Solutions. *Metall. Mater. Trans. B* **2021**, *52*, 3107–3119.
- (38) Wang, Z.; Halli, P.; Hannula, P.; Liu, F.; Wilson, B. P.; Yliniemi, K.; Lundström, M. Recovery of Silver from Dilute Effluents via Electrodeposition and Redox Replacement. *J. Electrochem. Soc.* **2019**, *166*, E266–E274.

- (39) Halli, P.; Elomaa, H.; Wilson, B. P.; Yliniemi, K.; Lundström, M. Improved Metal Circular Economy-Selective Recovery of Minor Ag Concentrations from Zn Process Solutions. *ACS Sustainable Chem. Eng.* **2017**, *5*, 10996–11004.
- (40) Molina, D. E.; Wall, N.; Beyenal, H.; Ivory, C. F. Flow Injection Electrochemical Quartz Crystal Microbalance with ICP-OES Detection: Recovery of Silver by Electrodeposition with Redox Replacement in a Flow Cell. *J. Electrochem. Soc.* **2021**, *168*, No. 056518.
- (41) Halli, P.; Wilson, B. P.; Hailemariam, T.; Latostenmaa, P.; Yliniemi, K.; Lundström, M. Electrochemical Recovery of Tellurium from Metallurgical Industrial Waste. *J. Appl. Electrochem.* **2020**, *50*, 1–14.
- (42) Halli, P.; Heikkinen, J. J.; Elomaa, H.; Wilson, B. P.; Jokinen, V.; Yliniemi, K.; Franssila, S.; Lundström, M. Platinum Recovery from Industrial Process Solutions by Electrodeposition–Redox Replacement. *ACS Sustainable Chem. Eng.* **2018**, *6*, 14631–14640.
- (43) Yliniemi, K.; Nguyen, N. T.; Mohajernia, S.; Liu, N.; Wilson, B. P.; Schmuki, P.; Lundström, M. A Direct Synthesis of Platinum/Nickel Co-Catalysts on Titanium Dioxide Nanotube Surface from Hydrometallurgical-Type Process Streams. *J. Cleaner Prod.* **2018**, *201*, 39–48.
- (44) Hannula, P.-M.; Pletincx, S.; Janas, D.; Yliniemi, K.; Hubin, A.; Lundström, M. Controlling the Deposition of Silver and Bimetallic Silver/Copper Particles onto a Carbon Nanotube Film by Electrodeposition-Redox Replacement. *Surf. Coat. Technol.* **2019**, *374*, 305–316.
- (45) Wang, Z.; Hannula, P.-M.; De, S.; Wilson, B. P.; Vapaavuori, J.; Yliniemi, K.; Lundström, M. Controllable Production of Ag/Zn and Ag Particles from Hydrometallurgical Zinc Solutions. *ACS Sustainable Chem. Eng.* **2021**, *9*, 8186–8197.
- (46) Laatikainen, K.; Lahtinen, M.; Laatikainen, M.; Paatero, E. Copper Removal by Chelating Adsorption in Solution Purification of Hydrometallurgical Zinc Production. *Hydrometallurgy* **2010**, *104*, 14–19.
- (47) Ahmed, I. M.; El-Nadi, Y. A.; Daoud, J. A. Cementation of Copper from Spent Copper-Pickle Sulfate Solution by Zinc Ash. *Hydrometallurgy* **2011**, *110*, 62–66.
- (48) Owusu, G. Selective Extraction of Copper from Acidic Zinc Sulfate Leach Solution Using LIX 622. *Hydrometallurgy* **1999**, *51*, 1–8.
- (49) Agarwal, S.; Ferreira, A. E.; Santos, S. M. C.; Reis, M. T. A.; Ismael, M. R. C.; Correia, M. J. N.; Carvalho, J. M. R. Separation and Recovery of Copper from Zinc Leach Liquor by Solvent Extraction Using Acorga M5640. *Int. J. Miner. Process.* **2010**, *97*, 85–91.
- (50) Zuo, Y.; Wang, K.; Pei, P.; Wei, M.; Liu, X.; Xiao, Y.; Zhang, P. Zinc Dendrite Growth and Inhibition Strategies. *Mater. Today Energy* **2021**, *20*, No. 100692.
- (51) Popov, K. I.; Nikolić, N. D. General Theory of Disperse Metal Electrodeposits Formation. In *Electrochemical Production of Metal Powders*; Djokić, S. S., Ed.; Springer: Boston, MA, 2012; Vol. 54, pp 1–62.
- (52) Park, H.; Choi, J.; Kim, H.; Hwang, E.; Ha, D.-H.; Ahn, S. H.; Kim, S.-K. AgIn Dendrite Catalysts for Electrochemical Reduction of CO<sub>2</sub> to CO. *Appl. Catal., B* **2017**, *219*, 123–131.
- (53) Gomes, A.; Viana, A. S.; da Silva Pereira, M. I. Potentiostatic and AFM Morphological Studies of Zn Electrodeposition in the Presence of Surfactants. *J. Electrochem. Soc.* **2007**, *154*, No. D452.
- (54) Xu, S.; Zhu, Y.; Xiong, D.; Wang, L.; Yang, P.; Chu, P. K. Zinc Electrodeposition on Polycrystalline Copper: Electrochemical Study of Early-Stage Growth Mechanism. *J. Phys. Chem. C* **2017**, *121*, 3938–3946.
- (55) Achari, I.; Ambrozik, S.; Dimitrov, N. Electrochemical Atomic Layer Deposition by Surface Limited Redox Replacement of Pd Thin Films in One-Cell Configuration Using Cu UPD Layers: Interrupting Mass-Transport Limited Growth. *J. Electrochem. Soc.* **2018**, *165*, J3074–J3082.
- (56) Fayette, M.; Liu, Y.; Bertrand, D.; Nutariya, J.; Vasiljevic, N.; Dimitrov, N. From Au to Pt via Surface Limited Redox Replacement of Pb UPD in One-Cell Configuration. *Langmuir* **2011**, *27*, 5650–5658.
- (57) Nutariya, J.; Fayette, M.; Dimitrov, N.; Vasiljevic, N. Growth of Pt by Surface Limited Redox Replacement of Underpotentially Deposited Hydrogen. *Electrochim. Acta* **2013**, *112*, 813–823.
- (58) Mitchell, C.; Fayette, M.; Dimitrov, N. Homo- and Hetero-Epitaxial Deposition of Au by Surface Limited Redox Replacement of Pb Underpotentially Deposited Layer in One-Cell Configuration. *Electrochim. Acta* **2012**, *85*, 450–458.
- (59) Ambrozik, S.; Dimitrov, N. The Deposition of Pt via Electroless Surface Limited Redox Replacement. *Electrochim. Acta* **2015**, *169*, 248–255.
- (60) Viyanalage, L. T.; Vasilic, R.; Dimitrov, N. Epitaxial Growth of Cu on Au(111) and Ag(111) by Surface Limited Redox Replacement. An Electrochemical and STM Study. *J. Phys. Chem. C* **2007**, *111*, 4036–4041.
- (61) Bauer, E.; van der Merwe, J. H. Structure and Growth of Crystalline Superlattices: From Monolayer to Superlattice. *Phys. Rev. B* **1986**, *33*, 3657–3671.